Project Report

Marco Savastano
Carmine Vardaro

Information Engineering for Digital Medicine
Artificial Intelligence for Omics Data Analysis Course 2025-2026

Contents

Abstract

The project is mainly focused on using LC-MS plasma metabolomics to address the identification of non-invasive maternal potential biomarkers for Congenital Heart Disease (CHD). The core was optimizing a robust workflow, by systematically evaluating pre-processing strategies, to prepare the dataset for prdictive models, in pursuance of the research of metabolic alteration associated with fetal CHD risk.

1 Introduction

1.1 Clinical background

The Congenital Heart Disease (CHD) corresponds to the most prelevant class of congenital anomalies, representing in pediatric morbidity and mortality a significant burden. Current prenatal diagnostic methods are mostly operator-depandant and may be faulty during early stages of gestation. Therefore, the importance in finding a non-invasive biomarker material which can facilitate early risks assesments, is critical in view of improving screening accuracy. The analysis of maternal plasma, can result and offer an interesting window into the complex biochemical environment of the growing fetus, in revealing of the metabolic disregulation associated with CHD pathogenesis which can exceeds solely genetic factors.

1.2 Untargeted metabolomic

A powerful analytical approach for phenotype characterization is the untargeted metabolomic, able to acquire the downstream end-products of genomic, transcriptomic, and proteomic processes. Opposing to target assays that quantify a limited list of pre-defined compounds, the main intent of untargeted Liquid Chromatography-Mass Spectrometry (LC-MS) is to ensure an exhaustive profile of small molecules with biological sample in a hypothesis-free manner. From an holistic perspective, this technique can result in becaming a considerable advantage in the investigation of complex pathologies such as CHD, where some more specific metabolic pathways may not be fully understood. By obtaining data in both positive (ESI+) and negative (ESI-) ionization modes, there is the capability of an unbiased detection of a diverse range of chemical classes and providing a detailed snapshot of the maternal metabolic phenotype (metabotype).

1.3 Open problematics

The high dimensionality and complexity of biological variance of the output of the LC-MS data places a significant computational challenge for the analysis. The primary notable issue is the absence of a gold standard for data pre-processing, critically influence the validity of downstream biological conclusions. Sometimes however, this absence can result in a more advantageous scenario, allowing for more accurate and tailored data preparation in view of the problem at hand. Systematic technical variations, such as sample dilution effects or instrumental fluctuations, has to be revised without removing genuine biological heterogeneity. Furthermore, the dataset composition and structure necessitate effective strategies, remining a complex analytical hurdle addressed in this project.

1.4 Project goal

The primary objective of this work is to delineate, evaluate and optimize a comprehensive chemiometric analysis workflow of the metabolomic plasma, in the context of CHD. One of the project intent was systematically asses and comparing the impact of different pre-processing strategies, to determine the best strategy for minimizing technical variance while preserving biological signal. Additionally, the application of Data Fusion techniques was utilized to integrate ESI+ and ESI- modalities, thereby exploiting their complementarity. Ultimately, the machine learning models were emloyed to determine and discriminate between healthy and pathological pregnancies and to identify statistically significant metabolic features that may serve as potential clinical biomarkers.

2 Materials and Methods

2.1 Dataset description

The dataset is composed of plasma metabolomic data derived from a cohort of pregnant women and acquired using Liquid Chromatography-Mass Spectrometry (LC-MS). The analysis was performed in both positive (ESI+) and negative (ESI-) ionisation mode, to guarantee a suffcient metabolic coverage. The dataset is divided into different distinct classes: decl

- CTRL (Control) samples related to mother of healty children
- CHD for Congenital Heart Disease pathologic cases
- QC (Quality Control) samples for each ionization mode, prepared by pooling equal fractions of all biological samples injected periodically to monitor instrumental stability and ensure analytical reproducibility.

The high-dimensionality data blocks are composed with metabolites on each row and indiviual bioligal samples on the columns. There are no missing values and zeros, due to a value inputation phase already done focused on the replacement with one-fifth of the minimum value recorded in the dataset for that molecule. [1]

The following tables give an overview on the dataset composition, for both ESI+ and ESI- with the corresponding values:

TABLE I: ESI- Dataset Distribution and Characteristics

DESCRIPTION	VALUE
Total Samples	219
Total Features (Metabolites)	52
Class Count: CTRL	107
Class Count: CHD	104
Class Count: QC	8
Samples with suffix '_00'	28
Samples with suffix '_01' (Tech Replicate)	14
Samples without suffix	177
Estimated Unique Biological Samples	205
CTRL - Biological Samples	100
CTRL - Technical Replicates	7
CHD - Biological Samples	97
CHD - Technical Replicates	7
QC - Total Samples	8
Negative Values Present	No

TABLE II: ESI+ Dataset Distribution and Characteristics

DESCRIPTION	VALUE
Total Samples	219
Total Features (Metabolites)	98
Class Count: CTRL	107
Class Count: CHD	104
Class Count: QC	8
Samples with suffix '_00'	28
Samples with suffix '_01' (Tech Replicate)	14
Samples without suffix	177
Estimated Unique Biological Samples	205
CTRL - Biological Samples	100
CTRL - Technical Replicates	7
CHD - Biological Samples	97
CHD - Technical Replicates	7
QC - Total Samples	8
Negative Values Present	No

2.2 Quality Assessment and Data Cleaning

This preliminary phase is crucial to validate the technical quality of the experiment before proceeding with biological interpretation.

To this end, we monitored the behavior of Quality Control (QC) samples (pooled aliquots injected periodically) and technical replicates (samples analyzed in duplicate, denoted with suffixes _00 and _01). The evaluation was performed using Principal Component Analysis (PCA) applied separately to the raw data of Negative (ESI-) and Positive (ESI+) ionization modes. Autoscaling was applied prior to PCA to ensure all metabolites contributed equally to the model, regardless of their absolute intensity.

PCA was employed as an unsupervised exploratory technique to visualize the intrinsic structure of the data variance. To facilitate the inspection of instrumental stability and technical reproducibility, specific sub-plots were generated from the same global PCA model to isolate QC samples and technical replicates. The results for the Negative and Positive ionization modes are presented in Figure 1 and Figure 2, respectively.

a) Variance and Model Structure

The Scree Plots (Fig. 1c, 2c) display the percentage of variance explained by each Principal Component (PC). The Loadings Plots (Fig. 1b, 2b) and Profiles (Fig. 1d-e, 2d-e) provide an overview of the features driving the separation.

b) Instrumental Stability (QC Analysis)

The stability of the LC-MS system was evaluated by isolating the QC samples in the PCA space. As shown in the QC-specific score plots (Fig. 1f, 2f), only the QC samples are visualized to assess their compactness. In the **Negative Ionization mode (ESI-)**, the QCs form a tight, well-defined cluster, indicating high instrumental stability. In the **Positive Ionization mode (ESI+)**, the QCs show a slightly higher dispersion. This behavior is attributed to the inherent characteristics of Hydrophilic Interaction Liquid Chromatography (HILIC). The HILIC separation mechanism relies on a water-enriched layer on the stationary phase, making the partitioning equilibrium more sensitive to minor fluctuations in column conditioning compared to reversed-phase chromatography. However, despite this inherent dispersion, the QC cluster remains distinct from the biological variability.

c) Technical Reproducibility (Replicates Analysis)

Reproducibility was assessed by projecting the technical replicates onto the PCA space (Fig. 1g, 2g). In these plots, non-replicated samples are hidden to highlight the distance between paired measurements (_00 and _01). In both ionization modes, the pairs of replicates are projected in close proximity, often overlapping, confirming that the analytical workflow yields consistent results for the same biological sample.

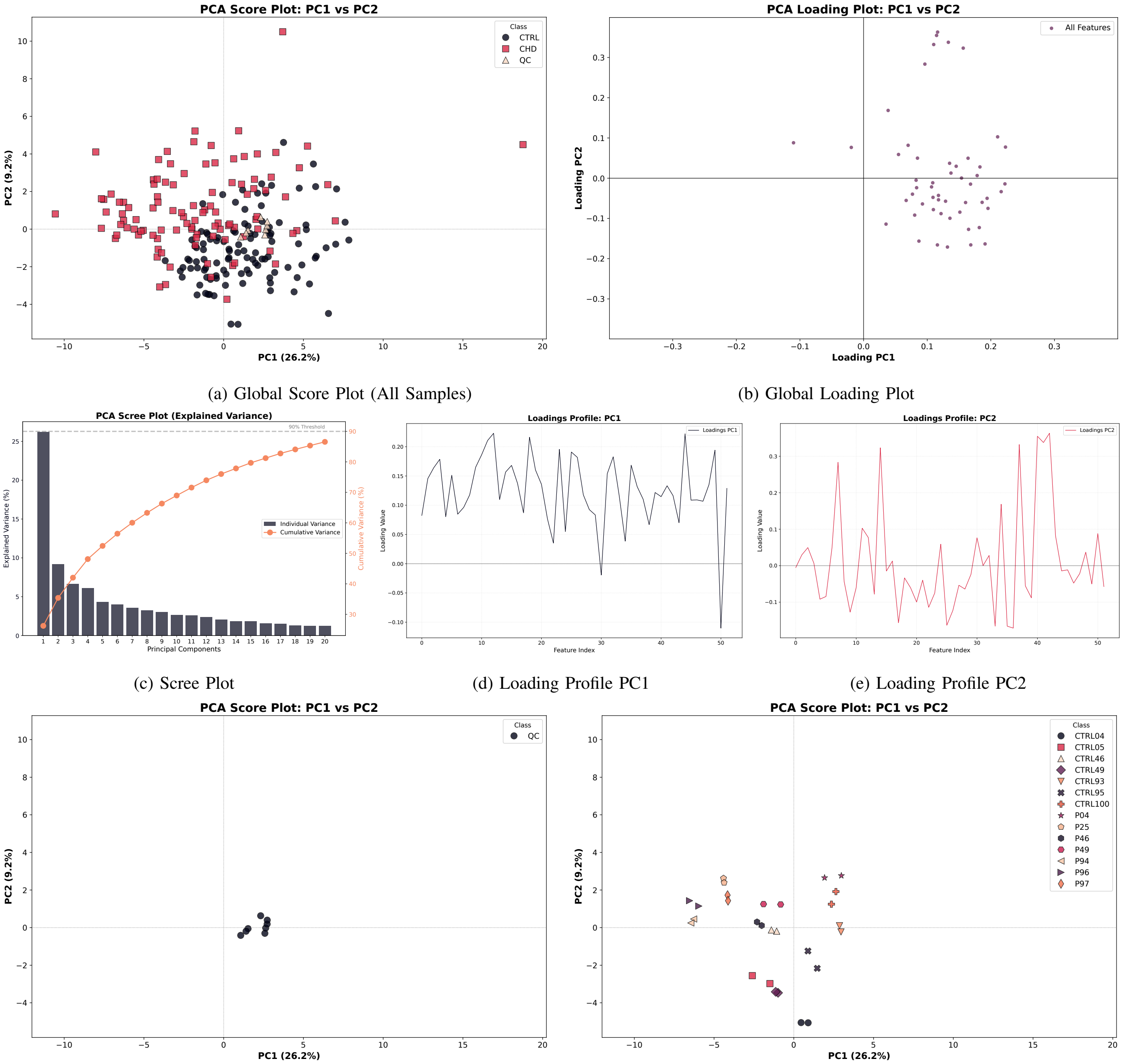

(a) Global Score Plot (All Samples)

(b) Global Loading Plot

(c) Scree Plot

(d) Loading Profile PC1

(e) Loading Profile PC2

(f) Instrumental Stability (QC only)

(g) Reproducibility (Replicates only)

Fig. 1: **Quality Assessment for ESI- Dataset.** (a) Global PCA Score plot showing the distribution of all classes (CHD, CTRL, QC). (b) Loading plot showing feature contributions. (c-e) Variance analysis and loading profiles. (f) Zoom on QC samples: the tight cluster confirms high stability. (g) Zoom on technical replicates: paired samples show high overlap, confirming reproducibility.

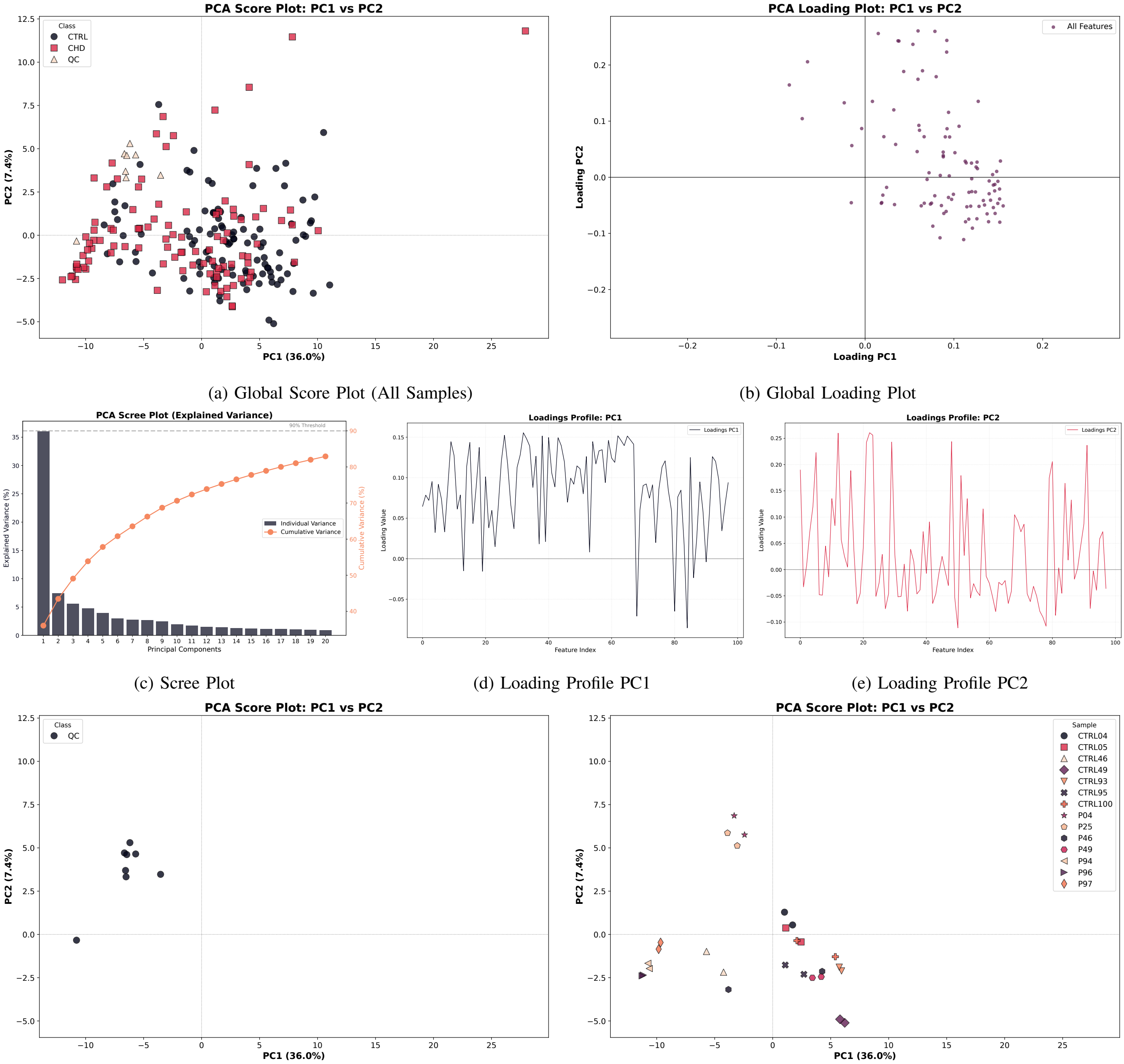

(a) Global Score Plot (All Samples)

(b) Global Loading Plot

(c) Scree Plot

(d) Loading Profile PC1

(e) Loading Profile PC2

(f) Instrumental Stability (QC only)

(g) Reproducibility (Replicates only)

Fig. 2: **Quality Assessment for ESI+ Dataset.** (a-b) Global PCA model overview. (c-e) Variance and Loadings. (f) Stability check: QCs show a wider dispersion compared to negative mode, consistent with HILIC sensitivity, but remain distinct from biological variance. (g) Reproducibility check showing paired replicates.

Having confirmed the technical robustness of the experiment, specific data cleaning steps were implemented to prepare the dataset for biological modeling.

d) Removal of Quality Control Samples

QC samples were removed from the final dataset as they have fulfilled their purpose of monitoring instrumental stability. Retaining QCs in downstream supervised analysis (e.g., PLS-DA) would introduce an artificial class that does not reflect a biological phenotype. Furthermore, due to their chemical homogeneity, QCs would form a dense cluster accounting for a large portion of the total variance, potentially masking the subtler biological differences between CHD and CTRL groups.

e) Removal of Technical Duplicates

To ensure the statistical independence of observations, technical duplicates were handled by retaining only one measurement per biological subject (samples with suffix _00). Including both replicates would violate the assumption of independence required by most statistical tests, artificially inflating the sample size and underestimating the intra-class variance. As duplicates were not available for all samples, averaging was avoided to prevent inconsistency in the data structure. Therefore, the removal of the second replicate (_01) ensures a homogeneous dataset where each sample represents a unique biological entity.

2.3 Data Pre-Processing

2.3.1 Data Normalization

The LC-MS untargeted analysis of biological fluids is inherently subject to systematic variations unrelated to the biological problem, such as differences in sample dilution (e.g., hydration status of the subjects) and fluctuations in ionization efficiency. As evidenced by the raw data distribution (Fig. 3a and Fig. 4a), a significant variability in the median intensity across samples was observed, necessitating a normalization step to render the samples comparable.

We evaluated multiple normalization strategies, ranging from global intensity corrections (TIC, Mean, Median) to distribution-based method (Quantile) and robust probabilistic approaches (Probabilistic Quotient Normalization - PQN). The selection of the optimal method was driven by a dual criterion: (i) qualitative inspection of sample distributions via boxplots, and (ii) quantitative assessment of the Coefficient of Variation (CV%) calculated on the technical replicates and across the biological groups.

Figures 3 and 4 illustrate the effect of selected normalization algorithms on the Negative (ESI-) and Positive (ESI+) datasets, respectively. While the raw data showed a pronounced ”batch-like” or dilution-related fluctuations, all normalization methods improved the alignment of sample medians. Specifically:

- **Total Ion Current (TIC):** Provided a standard correction based on the total signal sum, effectively reducing global differences but potentially sensitive to high-intensity artifacts.
- **Quantile Normalization:** Resulted in perfectly aligned distributions (Fig. 3c, 4c). However, visual inspection suggests this approach may be overly aggressive, forcing all samples to conform to an identical distribution and potentially suppressing genuine biological heterogeneity.
- **Probabilistic Quotient Normalization (PQN):** Demonstrated a robust alignment of medians and interquartile ranges (Fig. 3d, 4d) without imposing the artificial uniformity observed with Quantile normalization.

To objectively quantify the reduction in technical variance, the median Coefficient of Variation (CV%) was calculated for all features across the Control (CTRL) and Disease (CHD) groups. The results are summarized in Table III and Table IV.

In both ionization modes, normalization absence yielded the highest variability (Avg CV $\approx$ 58% for ESI- and 68% for ESI+). Consistent with the visual inspection, **Quantile normalization** achieved the lowest numerical CV values (Avg CV $\approx$ 50% and 57%, respectively). However, minimal variance is not solely indicative of data quality; it may also reflect overfitting and loss of biological signal. **PQN** consistently ranked among the top performing methods, achieving a substantial reduction in variance (Avg CV $\approx$ 51.5% for ESI- and 59.7% for ESI+) comparable to Quantile and Median normalization, while theoretically preserving the relative abundance ratios of metabolites better than global sum methods.

Based on the combined evidence, **PQN (Probabilistic Quotient Normalization)** was selected as the optimal strategy for this study. It provides the best trade-off between the reduction of systematic error (comparable to the most aggressive methods) and the preservation of biological variance required for the subsequent biomarker discovery phase.

TABLE III: Comparison of Normalization Methods by Coefficient of Variation (CV%) - ESI Negative Dataset.

Normalization Method	**Median CV CTRL (%)**	**Median CV CHD (%)**	**Average CV (%)**
Quantile	45.46	55.10	50.28
PQN	**44.94**	**58.06**	**51.50**
Mean / TIC	45.91	59.66	52.79
Median	45.48	63.94	54.71
Range / Max	51.28	63.22	57.25
None (Raw)	49.11	67.40	58.26

TABLE IV: Comparison of Normalization Methods by Coefficient of Variation (CV%) - ESI Positive Dataset.

Normalization Method	**Median CV CTRL (%)**	**Median CV CHD (%)**	**Average CV (%)**
Quantile	53.35	61.62	57.48
Median	54.48	60.69	57.58
Range / Max	53.84	64.46	59.15
PQN	**56.12**	**63.38**	**59.75**
Mean / TIC	54.44	65.09	59.77
None (Raw)	58.43	77.84	68.14

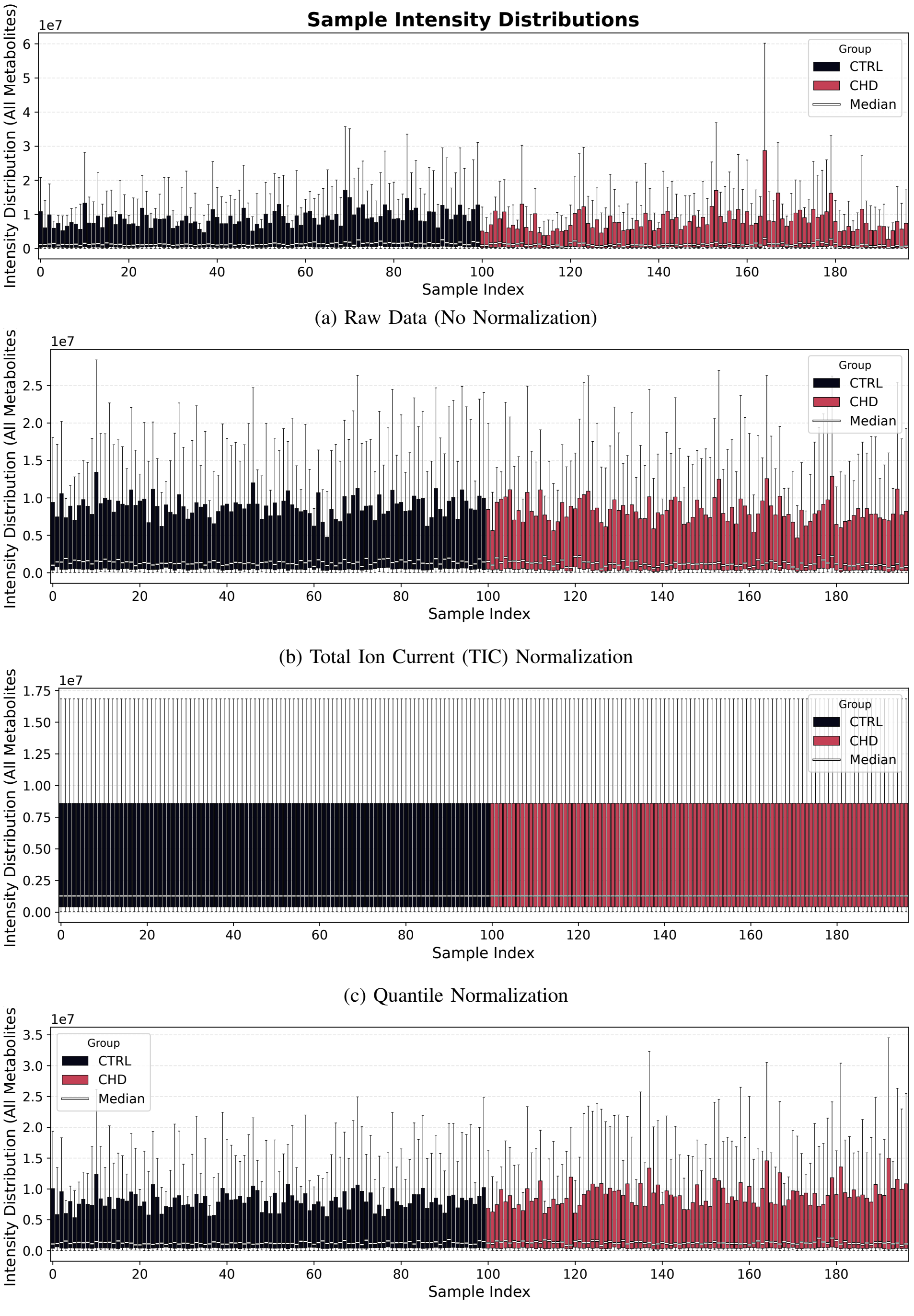

(a) Raw Data (No Normalization)

(b) Total Ion Current (TIC) Normalization

(c) Quantile Normalization

(d) Probabilistic Quotient Normalization (PQN)

Fig. 3: **Comparison of Normalization Strategies for ESI- Dataset.** Boxplots representing the global intensity distribution of all samples. (a) Raw data showing significant systematic variation (e.g., dilution effects). (b) TIC normalization, acting on the total sum. (c) Quantile normalization, forcing identical distributions potentially suppressing biological signal. (d) PQN, the selected method, which effectively reduces technical variance while preserving biological information.

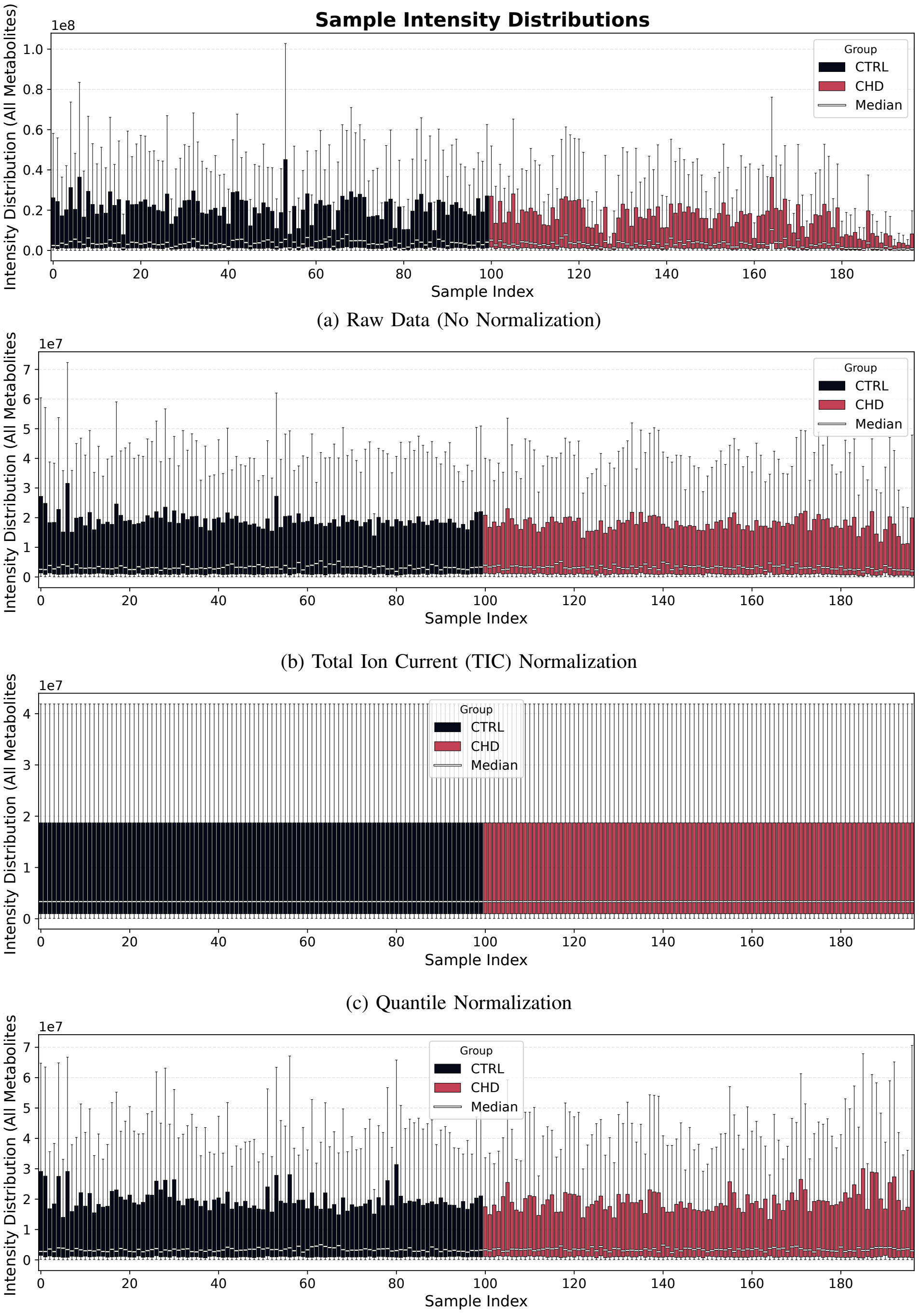

(a) Raw Data (No Normalization)

(b) Total Ion Current (TIC) Normalization

(c) Quantile Normalization

(d) Probabilistic Quotient Normalization (PQN)

Fig. 4: **Comparison of Normalization Strategies for ESI+ Dataset.** (a) Raw data distribution. (b) TIC normalization results. (c) Quantile normalization results showing aggressive distribution alignment. (d) PQN results, selected as the optimal compromise for downstream analysis.

2.3.2 Data Transformation

Following the normalization strategies assessment, the distribution of the intensity values was evaluated to satisfy the assumptions of normality required by multivariate statistical methods (e.g., PCA, PLS-DA) and parametric univariate tests (e.g., t-test). LC-MS metabolomics data typically exhibit a right-skewed distribution, where the majority of signals have low intensity, while a few highly abundant metabolites stretch the dynamic range, potentially dominating the variance [2].

It this project there were evaluated different variance-stabilizing transformations, including power transformations (Square Root, Cube Root) and logarithmic transformations (Log2, Natural Logarithm, Log10). Visual inspection of the global density plots revealed that power transformations were insufficient to correct the distribution's skewness. Conversely, all logarithmic transformations effectively compressed the high-intensity values and expanded the low-intensity range, resulting in a distribution approximating a Gaussian curve.

Since Log2, Ln, and Log10 produced equivalent distributional shapes differing only in scale, **Log10 transformation** was selected as the standard method for this study. This transformation is widely accepted in mass spectrometry as it renders orders of magnitude easily interpretable while effectively symmetrizing the data distribution.

Figure 5 and Figure 6 illustrate the comparative analysis between the non-transformed data and the Log10-transformed data for the ESI- and ESI+ datasets, respectively. In the transformed data, the empirical density (solid line) shows a significant overlap with the theoretical Gaussian distribution (dashed line), confirming the efficacy of the transformation.

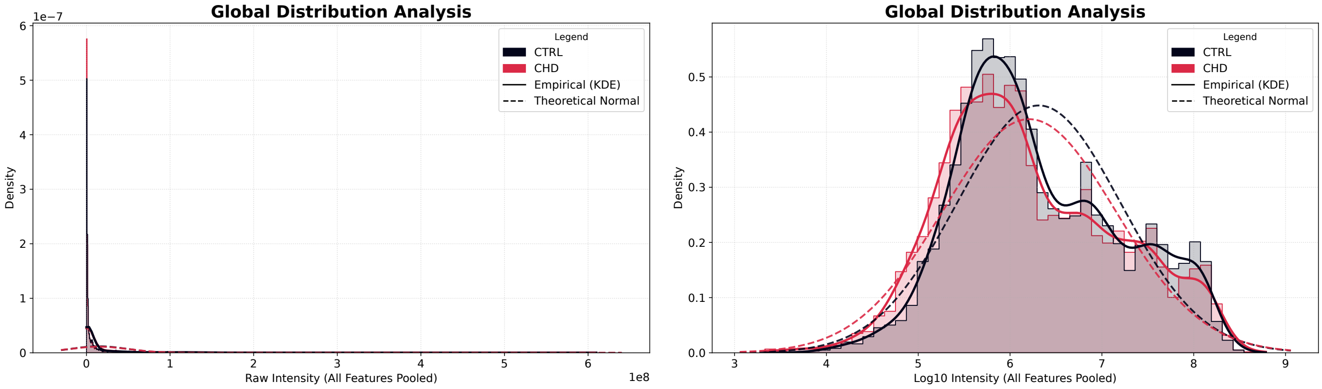

(a) Original Distribution (Skewed)

(b) After Log10 Transformation

Fig. 5: **Effect of Log10 Transformation on ESI- Dataset.** Global density plots pooling all feature intensities. (a) The original data distribution is highly right-skewed, deviating significantly from the theoretical normal distribution (dashed line). (b) Log10 transformation successfully centers the distribution, achieving a Gaussian-like shape suitable for multivariate analysis.

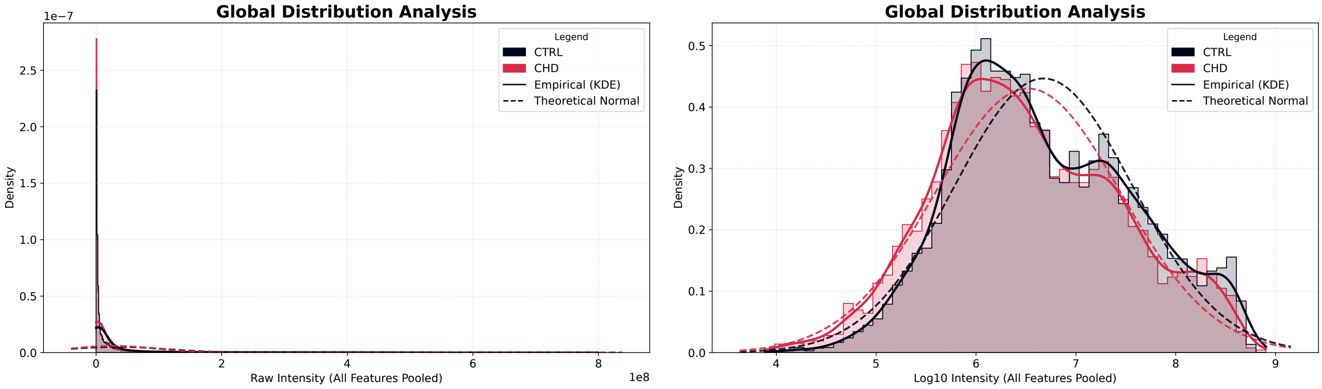

(a) Original Distribution (Skewed)

(b) After Log10 Transformation

Fig. 6: **Effect of Log10 Transformation on ESI+ Dataset.** (a) The raw positive mode data exhibits a pronounced right-skewness. (b) Log10 transformation corrects the skewness, aligning the empirical density (solid line) with the theoretical Gaussian curve (dashed line).

2.3.3 Data Scaling

The final step of the pre-processing pipeline involved data scaling. In metabolomics, metabolite intensities can span several orders of magnitude. Without proper scaling, variables with high abundance and large variance would naturally dominate multivariate models based on variance maximization (e.g., PCA), biasing the results and potentially masking significant biological variations present in low-abundance metabolites.

To address this issue, **Autoscaling** (Unit Variance Scaling) was applied to the normalized and transformed data. This method involves mean-centering each variable and dividing it by its standard deviation. As a result, all metabolites are scaled to have a mean of zero and a standard deviation of one, ensuring that each feature contributes equally to the statistical model regardless of its absolute concentration.

Figure 7 and Figure 8 demonstrate the effect of autoscaling on the feature distributions for ESI- and ESI+ datasets, respectively. Before scaling (Panel a), the variables exhibit disparate ranges of intensity. After autoscaling (Panel b), it is possible to cpare all features, centered around zero with standardized variance, making the dataset suitable for unsupervised and supervised modeling.

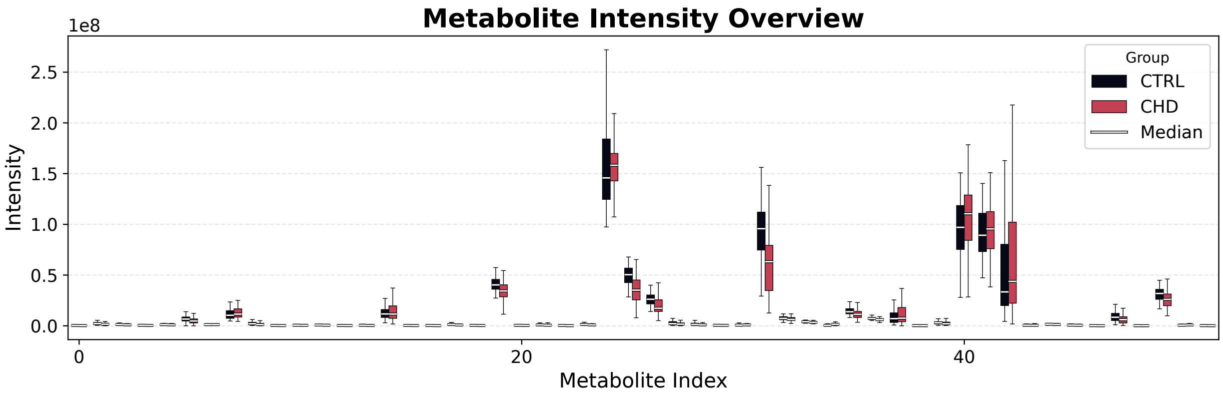

(a) Before Scaling (Variable Intensities)

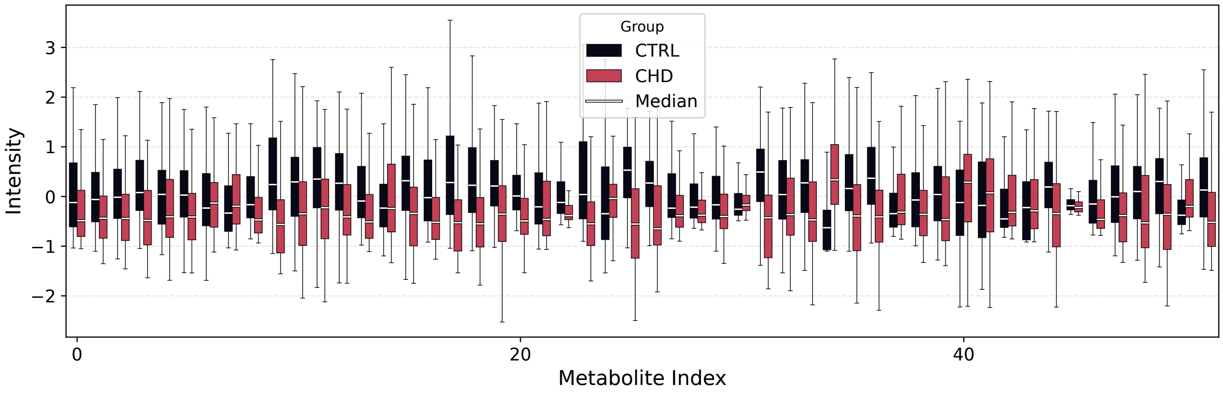

(b) After Autoscaling (Unit Variance)

Fig. 7: **Effect of Autoscaling on ESI- Features.** Boxplots representing the distribution of individual metabolites (features). (a) Original features show highly variable ranges and variances. (b) After autoscaling, all features are mean-centered with unit variance, ensuring equal weight in multivariate analysis.

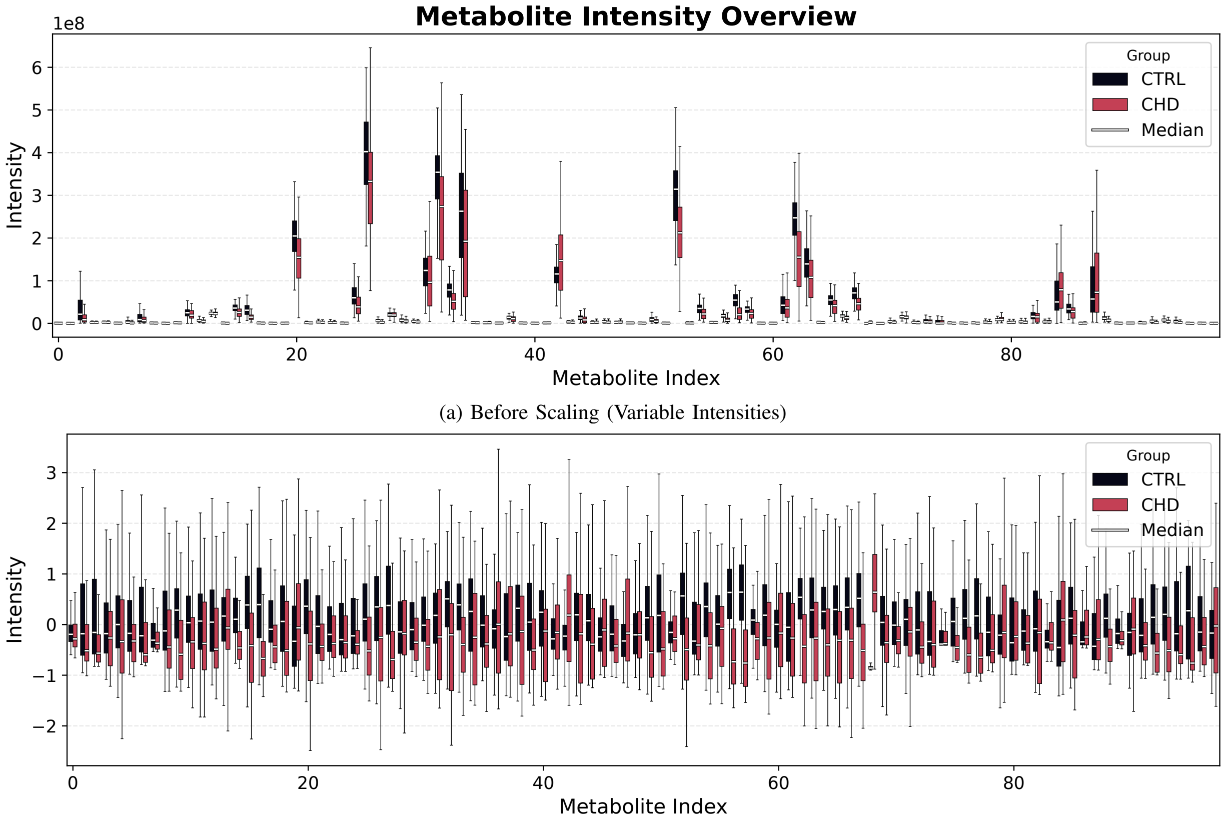

(a) Before Scaling (Variable Intensities)

(b) After Autoscaling (Unit Variance)

Fig. 8: **Effect of Autoscaling on ESI+ Features.** (a) The disparate scales of metabolite intensities in the positive mode. (b) The homogenized feature space achieved through autoscaling.

2.3.4 Global Assessment

To validate the efficacy of the entire pre-processing pipeline

- PQN normalization
- Log10 transformation
- Autoscaling

, a comparative Principal Component Analysis (PCA) was performed on the dataset before and after data pre-treatment. This step is essential to confirm that the applied corrections have successfully removed systematic bias and magnitude-dependent effects without distorting the biological signal.

Figure 9 illustrates the dramatic shift in data structure for the **Negative (ESI-) dataset**. In the **Raw Data** (Panels a-c), the variance is dominated by high-intensity compounds. The Loading Plot (c) shows that a restricted number of fatty acids (e.g., Palmitoleic acid, Oleic acid) possess extremely high loading values, driving more effectively the separation solely based on their abundance magnitude rather than biological class differences. Consequently, the Score Plot (b) shows a clustering pattern heavily influenced by these dominant features.

In the **Pre-processed Data** (Panels d-f), the variance is more evenly distributed across components (Scree Plot d), reflecting the effect impressed by the autoscaling processing, which gives equal weight to all metabolites. The Score Plot (e) reveals a more homogeneous distribution of samples centered at the origin. Crucially, the Loading Plot (f) now highlights a diverse range of metabolites (e.g., Indolelactic acid) contributing to the model, ensuring that the subsequent multivariate analysis searches for potential biomarkers across the entire dynamic range of the metabolome.

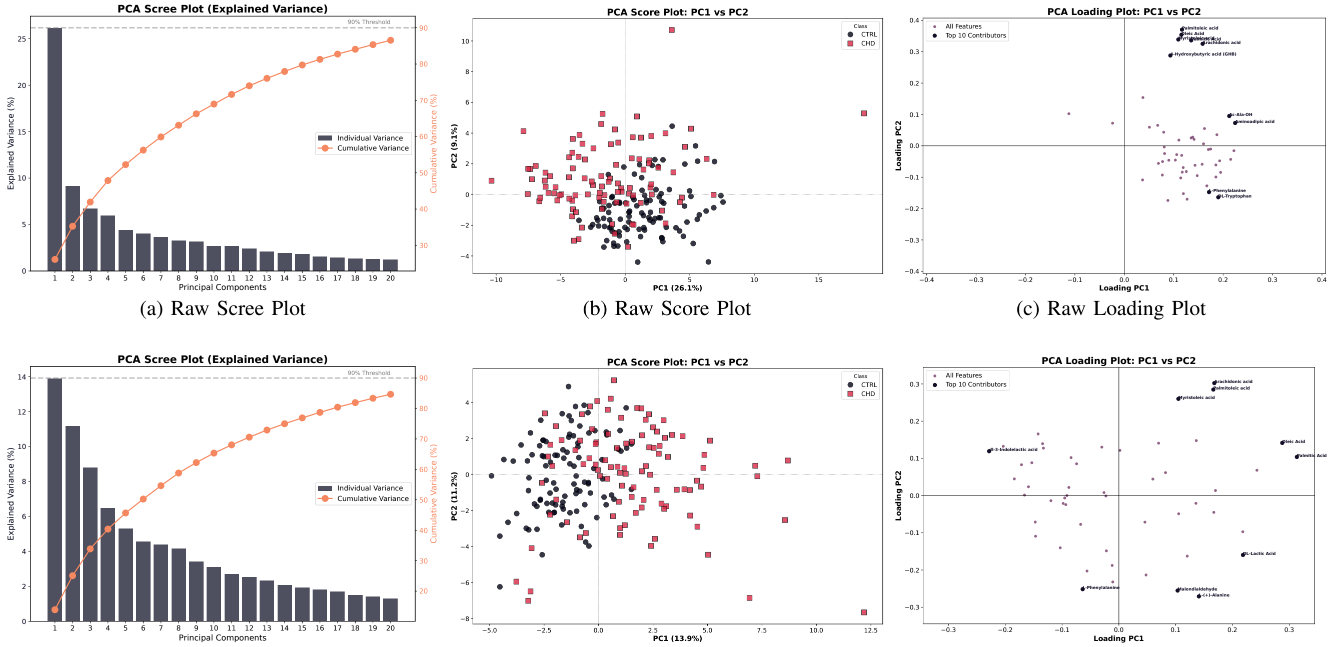

(a) Raw Scree Plot

(b) Raw Score Plot

(c) Raw Loading Plot

(d) Proc. Scree Plot

(e) Proc. Score Plot

(f) Proc. Loading Plot

Fig. 9: **Impact of Pre-processing on ESI- Data Structure. Top Row (a-c):** PCA on raw data. The model is dominated by high-abundance features (fatty acids) explaining a large portion of variance (26% on PC1), masking subtle biological signals. **Bottom Row (d-f):** PCA on pre-processed data (PQN + Log10 + Autoscaling). The variance is democratized, and the influence of dominant metabolites is rescaled, revealing a more complex biological structure suitable for biomarker discovery.

A similiar trend was observed for the **Positive (ESI+) dataset** (Figure 10). In the raw state (Panels a-c), the variance was heavily skewed by high-abundance lipid species, specifically medium-chain acylcarnitines (e.g., C8-Carnitine, Decanoylcarnitine). The Loading Plot (c) clearly indicates that the separation along PC1 was driven almost exclusively by the magnitude of these compounds. Following the application of the optimized pre-processing pipeline (Panels d-f), the variance distribution was normalized. The Loading Plot (f) shows a re-balancing of feature importance: while acylcarnitines remain relevant, other metabolite classes (e.g., indolic compounds like trans-3-Indoleacrylic acid) now contribute significantly to the model components. This confirms that the pre-processing successfully revealed the latent biological information previously masked by the dominant lipid signals.

Having an independently data quality optimization for both ionization modes, the separate processing workflows were concluded. To exploit the complementary nature of the ESI+ and ESI- profiles and capture comprehensive metabolic signatures, the next phase involves the integration of the two datasets. Specifically, a **Low-Level Data Fusion** strategy was be applied prior to outlier detection. This approach other than ensuring a more robust dataset for the final classification modeling, allows for the identification of potential anomalies, not only within a single analytical domain, but also arising from inconsistencies between the two ionization modes.

2.4 Low-Level Data Fusion

The **Low-Level Data Fusion** strategy was implemented in order to obtain a comprehensive metabolic phenotype view and exploit the complementary nature of the two ionization modes. This approach involves the concatenation of the pre-processed datasets into a single super-matrix, allowing for the simultaneous analysis of interactions between all variables.

a) Fusion Strategy and Block Scaling

Prior to concatenation, a critical **Block Scaling** step was performed to ensure fairness between the two analytical blocks (ESI- and ESI+). Although both datasets were individually autoscaled, differences in the number of variables (P) and the intrinsic numerical redundancy could lead to one block dominating the multivariate model. To prevent this, each block X_k was scaled by its Frobenius norm ($||X_k||_F$), defined as the square root of the sum of the squared elements:

$$X_{k,scaled} = \frac{X_k}{\sqrt{\sum_{i,j} x_{k,ij}^2}} \tag{1}$$

This operation normalizes the total variance (energy) of each matrix, ensuring that both ionization modes contribute equitably to the fused model. Subsequently, the blocks were concatenated horizontally to form the super-matrix $X_{fus} = [X_{neg}|X_{pos}]$, preserving the sample alignment.

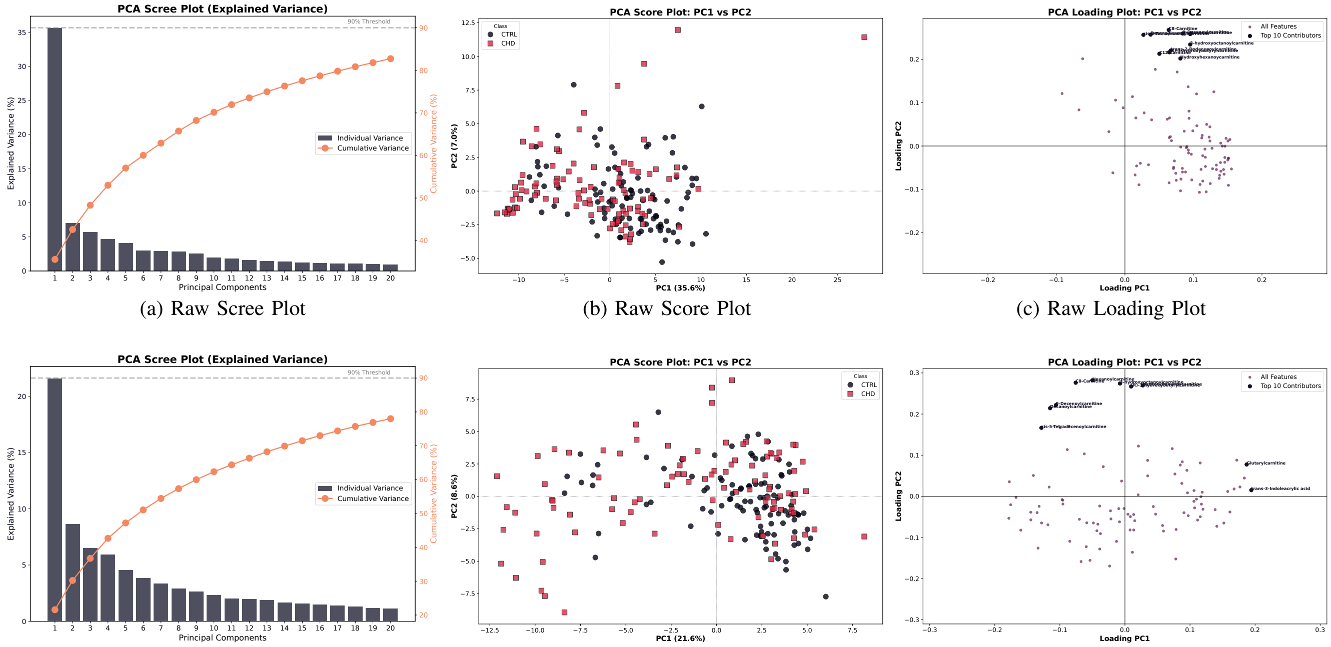

(a) Raw Scree Plot

(b) Raw Score Plot

(c) Raw Loading Plot

(d) Proc. Scree Plot

(e) Proc. Score Plot

(f) Proc. Loading Plot

Fig. 10: **Impact of Pre-processing on ESI+ Data Structure. Top Row (a-c):** PCA on raw data. The model is biased by high-intensity acylcarnitines. **Bottom Row (d-f):** PCA on pre-processed data. The influence of dominant lipids is rescaled, allowing for a more comprehensive representation of the metabolome, including amino acid derivatives and indoles.

b) SUM-PCA: Exploratory Analysis of Fused Data

Principal Component Analysis applied to the fused super-matrix (defined as **SUM-PCA**) was utilized to decompose the global variance into Super Scores (representing the consensus sample trajectory) and Super Loadings (representing the contribution of features from both blocks).

The results of the SUM-PCA are presented in Figure 11. The **Scree Plot (g)** reveals the variance contribution of each block to the principal components. A clear complementarity is observed: PC1 (13.8%) is predominantly driven by Block 2 (ESI+), indicating that the positive dataset accounts for the majority of the global variation. In contrast, PC2 (7.7%) and PC3 (7.2%) show a substantial recovery of contribution from Block 1 (ESI-), balancing the model.

The **Score Plots (a-c)** show the distribution of samples in the integrated latent space, suggesting a trend of biological distinction driven by the combined metabolic profile.

The **Super Loadings Plots (d-f)** provide insight into the specific features driving these components. Interestingly, while the Positive block dominates the global variance on PC1 (as seen in the Scree Plot), the top contributing features (highest loading values) identified in the plots belong primarily to the **Negative Block (ESI-)**.

- **PC1 vs PC2 (d):** The loading space is characterized by high-ranking negative mode metabolites, including fatty acids like Oleic Acid and Palmitic Acid, and polar compounds such as Uric Acid. This suggests that while the Positive block provides the ”bulk” of the information, specific Negative block markers are highly specific and hold the strongest weights in defining the sample separation along these axes [3].
- **PC3 contributions:** The third component is similarly heavily influenced by specific markers from the Negative dataset, such as Arachidonic Acid and amino acid derivatives (e.g., L-Phenylalanine), further confirming the crucial role of ESI- features in characterizing the fine structure of the data.

This integrated analysis demonstrates that Low-Level Fusion successfully combined the broad variance coverage of the ESI+ mode with the high feature specificity of the ESI- mode.

2.5 Anomaly Detection

Following data fusion, a rigorous anomaly detection phase was conducted to identify samples presenting extreme deviant behaviors or technical artifacts. This step was performed on the **Low-Level Fused dataset** to capture potential inconsistencies arising either from a single ionization mode and from the interaction between the two platforms (e.g., a sample appearing normal in ESI- but aberrant in ESI+).

Crucially, the detection was performed **independently for each class** (CTRL and CHD). This stratified approach ensures the definition of a normal situation which respects the specific biological topology of each group and preventing the algorithm from flagging a genuine pathological variation as a technical outlier.

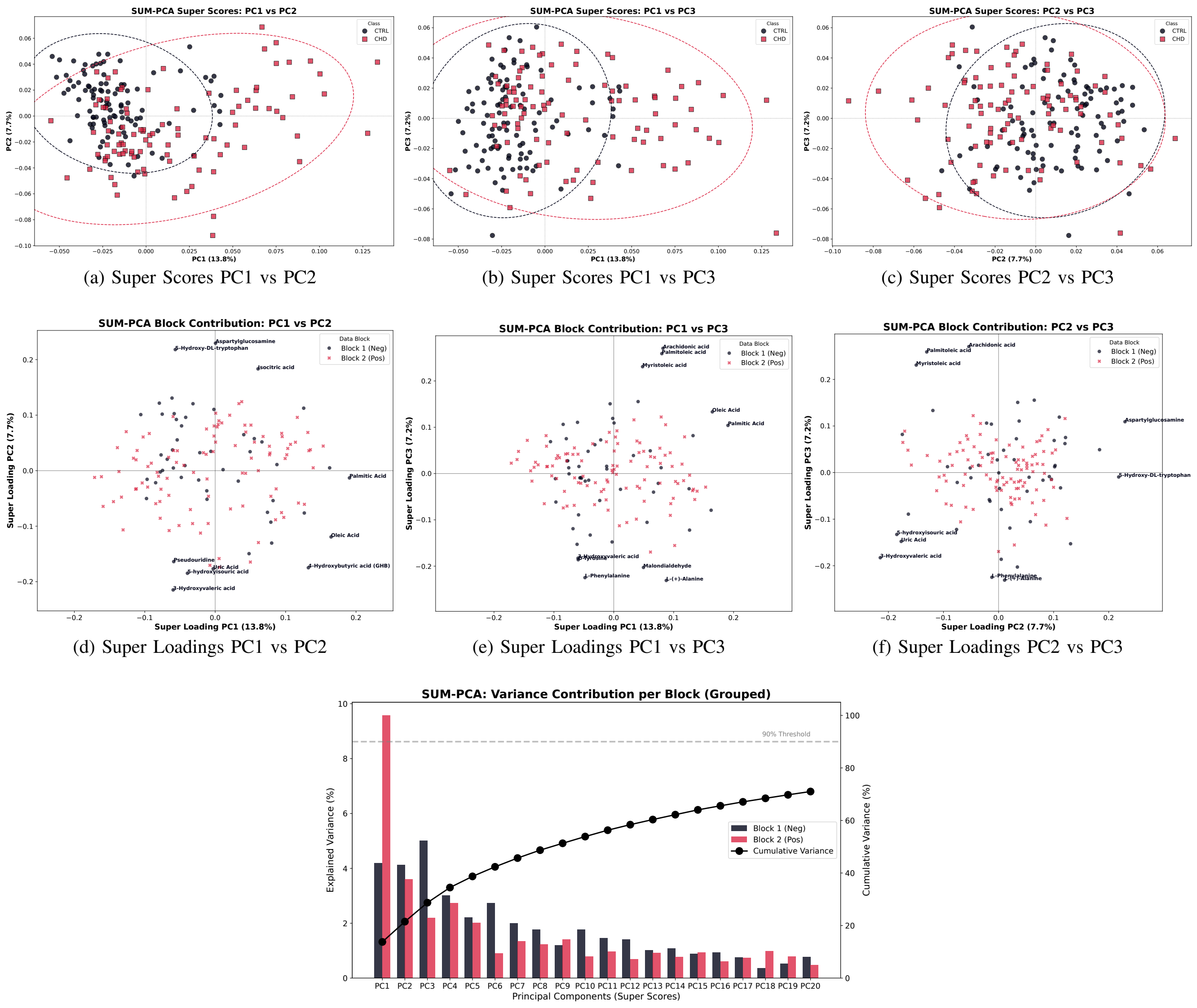

(a) Super Scores PC1 vs PC2 (b) Super Scores PC1 vs PC3 (c) Super Scores PC2 vs PC3

(d) Super Loadings PC1 vs PC2 (e) Super Loadings PC1 vs PC3 (f) Super Loadings PC2 vs PC3

(g) Variance Contribution per Block (Scree Plot)

Fig. 11: **SUM-PCA Results on Low-Level Fused Data.** (a-c) Super Score plots showing sample distribution in the integrated space. (d-f) Super Loading plots. Notably, despite the high global variance of the Positive block, the top ranking contributors (labeled features) are primarily from the **ESI- Block** (e.g., Palmitic Acid, Uric Acid), highlighting their specific relevance. (g) Scree plot highlighting the variance contribution: PC1 is dominated by Block 2 (Pos), while subsequent components show increased contribution from Block 1 (Neg).

A multi-methodological consensus strategy was adopted, combining multivariate statistics and machine learning algorithms to evaluate the samples from different topological perspectives (distance, density, and isolation).

a) Multivariate Statistical Profiling

First, Principal Component Analysis (PCA) was used to define the boundaries of the model space. Two complementary metrics were calculated for each sample:

- **Hotelling's T^2:** Measures the distance of a sample from the center of the model within the orthogonal subspace defined by the Principal Components (PCs). It identifies ”extreme” samples that follow the model but possess exaggerated leverage.
- **Q-Residuals (Squared Prediction Error):** Measures the distance of a sample from the model plane (i.e., the error between the raw data and the PCA reconstruction). It identifies samples with a chemical composition inconsistent with the correlation structure of the majority.

To ensure mathematical robustness, the number of PCs used for the T^2 calculation was dynamically selected to explain 90% of the variance, respecting the degrees of freedom constraints.

b) Machine Learning-Based Detection

To complement the statistical metrics, three unsupervised Machine Learning algorithms were deployed. The input space for these models was carefully selected to mitigate the ”Curse of Dimensionality”:

1) **Isolation Forest (iForest):** Applied directly to the **Raw Fused Data**. Since iForest relies on random partitioning rather than distance calculations, it is intrinsically robust to high-dimensional spaces. It identifies anomalies as points that are ”few and different,” requiring fewer random splits to be isolated from the rest of the data.
2) **One-Class SVM (OC-SVM):** Applied to the **PCA Scores (95% variance)**. This algorithm maps the data into a high-dimensional feature space using an RBF kernel to find the smallest hypersphere enclosing the ”normal” observations ($\nu = 0.05$). The use of PCA scores ensures the model focuses on biological variance rather than noise.
3) **Local Outlier Factor (LOF):** Applied to the **PCA Scores (95% variance)**. Unlike the global approach of iForest and OC-SVM, LOF evaluates the local density of a sample compared to its k-nearest neighbors ($k = 20$). It is particularly effective at identifying samples located in sparse regions or at the edges of the class cluster.

c) Visualization of Decision Boundaries

To visually interpret the behavior of the ML algorithms, the decision boundaries were projected onto the first two Principal Components (Figure 12 and Figure 13). From this plots it is possible to appreciate and identify the different topological assumptions of the methods: **iForest** and **OC-SVM** define a global envelope around the core distribution, while **LOF** adapts to the local density variations.

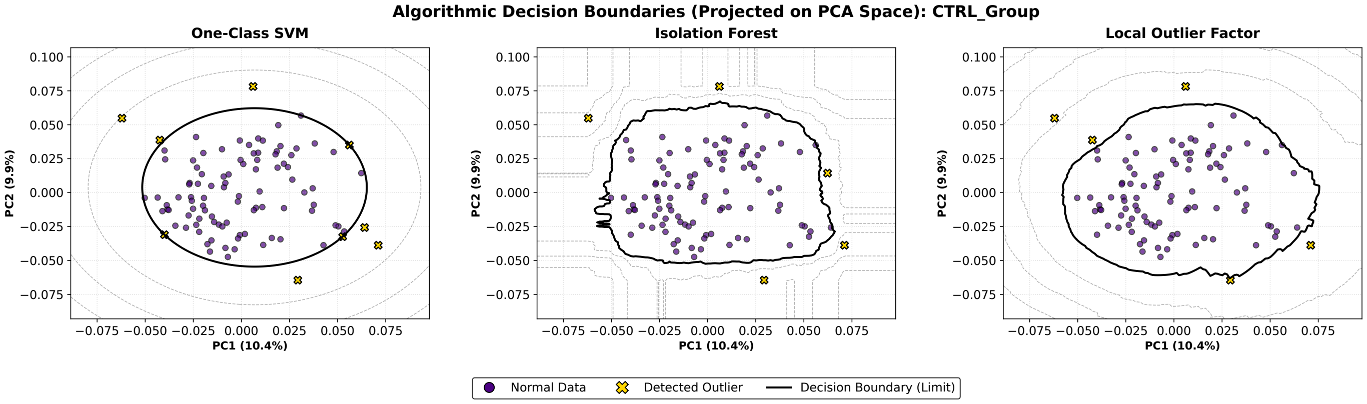

Fig. 12: **Algorithmic Decision Boundaries for Control Group (CTRL).** 2D projection of the decision boundaries generated by One-Class SVM, Isolation Forest, and Local Outlier Factor on the Control dataset. The colored regions and contours illustrate the area considered ”normal” by each algorithm. Samples falling outside these boundaries (marked with ’X’) are flagged as potential outliers. Note that actual detection was performed in the high-dimensional space (or raw space for iForest) to preserve information; this 2D representation is for visualization of the topological approach only.

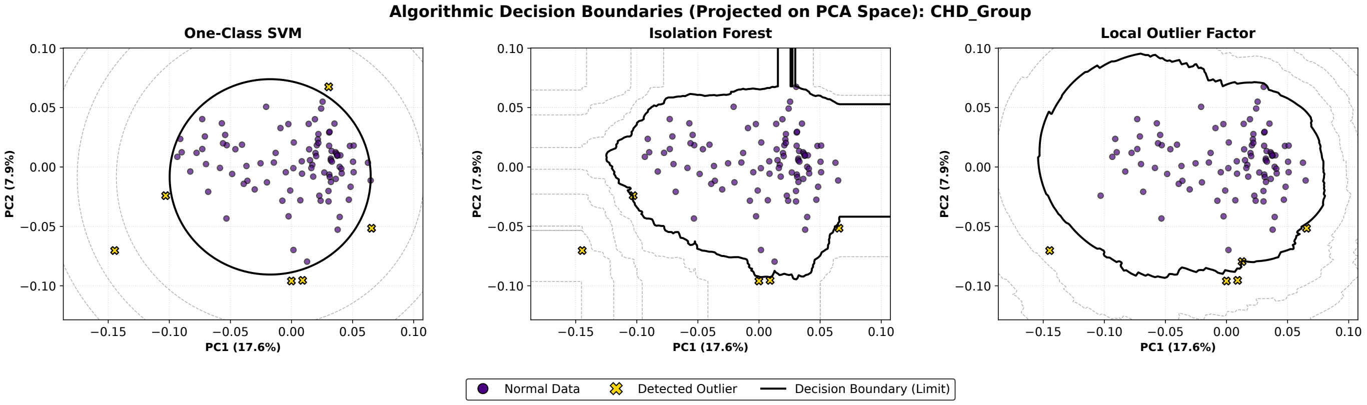

Fig. 13: **Algorithmic Decision Boundaries for Disease Group (CHD).** Visualization of anomaly detection results for the CHD class. The algorithms successfully identify samples that deviate from the main distribution cluster. The consensus among these methods, combined with the statistical metrics (T^2 and Q), forms the basis for the final exclusion criteria.

d) Consensus Evaluation and Sample Filtering

Since the primary objective of omics studies is to identify robust potential biomarkers, the exclusion of samples must be carefully balanced to avoid reducing statistical power while ensuring data quality. A consensus approach was adopted, integrating the multivariate metrics (T^2 vs Q) with the alerts generated by the Machine Learning algorithms and a visual inspection of the intensity distributions.

The **Distance Plots** (Figure 14) provide a exhaustive view of the outlier candidates. Notably, the majority of flagged samples exhibited high **Q-Residuals** (y-axis), indicating a significant deviation from the correlation structure of the model, also known as Model Mismatch, likely due to technical artifacts or qualitative inconsistencies in sample composition. Conversely, no extreme biological outliers (high T^2) were detected in the Control group, whereas the CHD group showed specific deviant behaviors.

To validate these statistical alerts, the raw intensity distributions of the candidate samples were inspected via **Boxplots** (Figure 15 and Figure 16). This step was decisive for borderline cases.

- **Confirmed Exclusions:** Samples *CTRL09_00*, *CTRL93_00*, and *CTRL41* were removed due to severe violation of the Q-residuals limit. Similarly, *CTRL60*, *CTRL02_00*, and *CTRL53* were excluded as their statistical anomaly was corroborated by visible distributional artifacts in the boxplots. In the pathological group, *P06_00*, *P42*, and *P59* were removed for high Q-residuals. Sample *P93* was excluded as a unique ”biological outlier,” being unanimously flagged by all Machine Learning algorithms (iForest, SVM, LOF) and located at the extreme of the model space (T^2).
- **Saved Samples:** Sample *CTRL13*, despite having a Q-residual value near the threshold, was retained. Its raw intensity profile appeared consistent with the healthy population distribution, suggesting that the statistical deviation was not sufficient to justify data loss.

In total, **10 samples** (approx. 5% of the dataset) were removed: *CTRL02_00, CTRL09_00, CTRL41, CTRL53, CTRL60, CTRL93_00* from the Control group, and *P06_00, P42, P59, P93* from the CHD group.

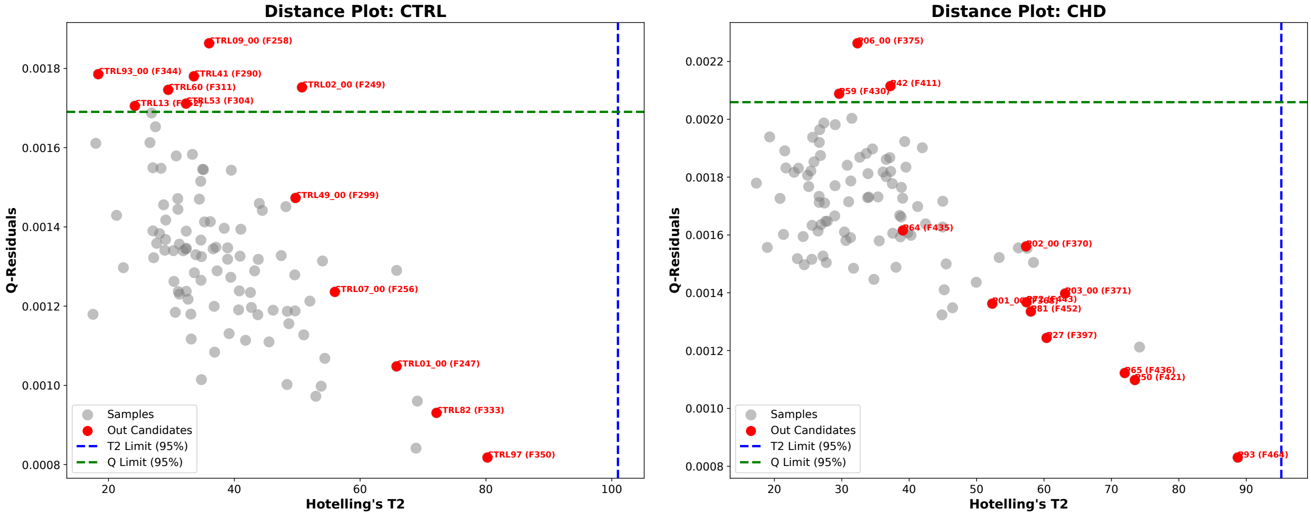

(a) Control Group

(b) CHD Group

Fig. 14: **Distance Plots** (T^2 **vs** Q**-Residuals).** Gold standard visualization for outlier diagnosis. Samples flagged by at least two Machine Learning algorithms are highlighted in red. (a) Controls show anomalies primarily in the Q-residual space (vertical axis), indicating technical mismatch. (b) CHD samples show a more complex pattern, with sample P93 appearing as a distinct outlier consistent with ML detection.

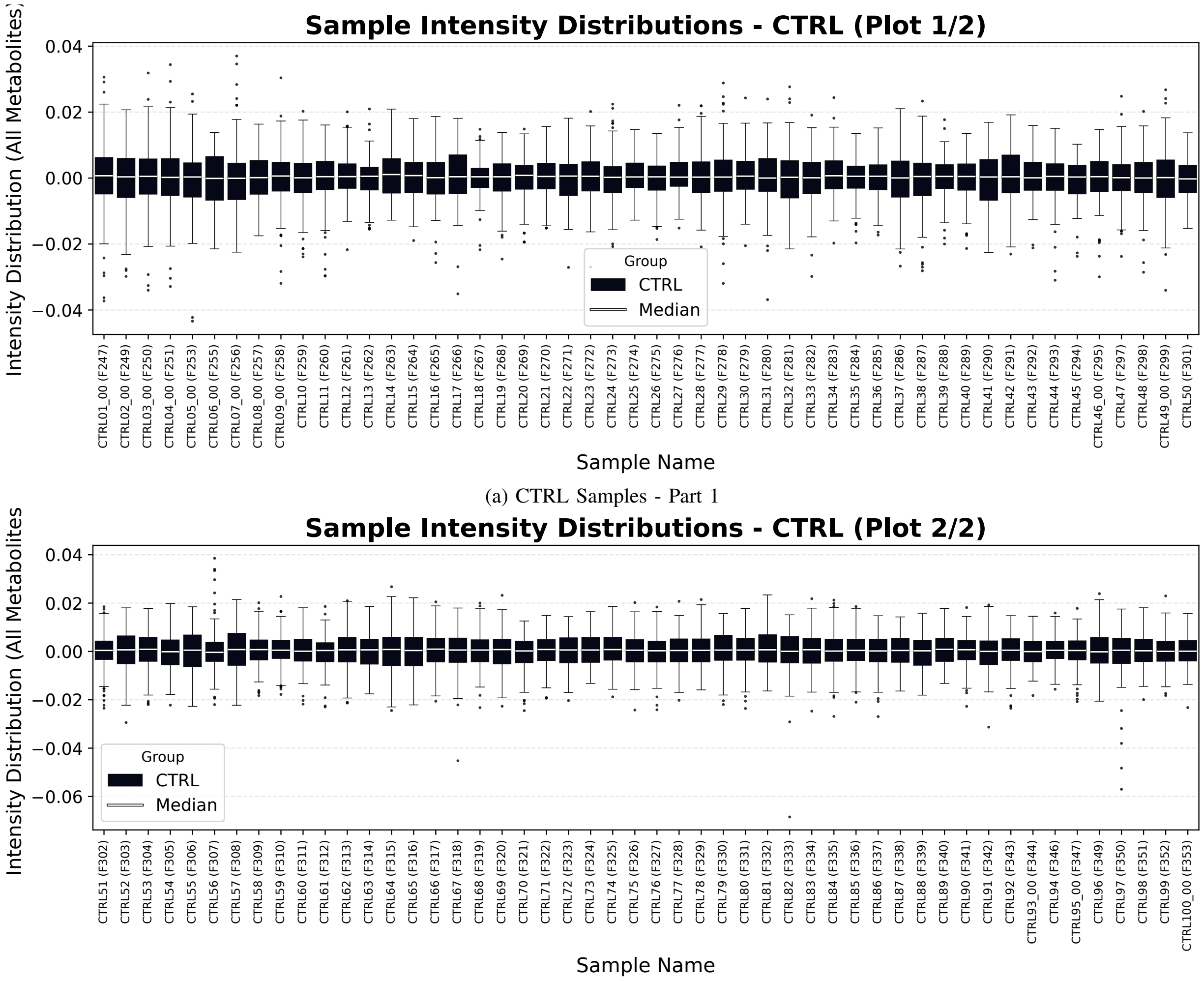

(a) CTRL Samples - Part 1

(b) CTRL Samples - Part 2

Fig. 15: **Intensity Distributions of Control Samples.** Visual inspection used to validate statistical outliers. Deviant distributions confirmed the exclusion of samples like CTRL02_00.

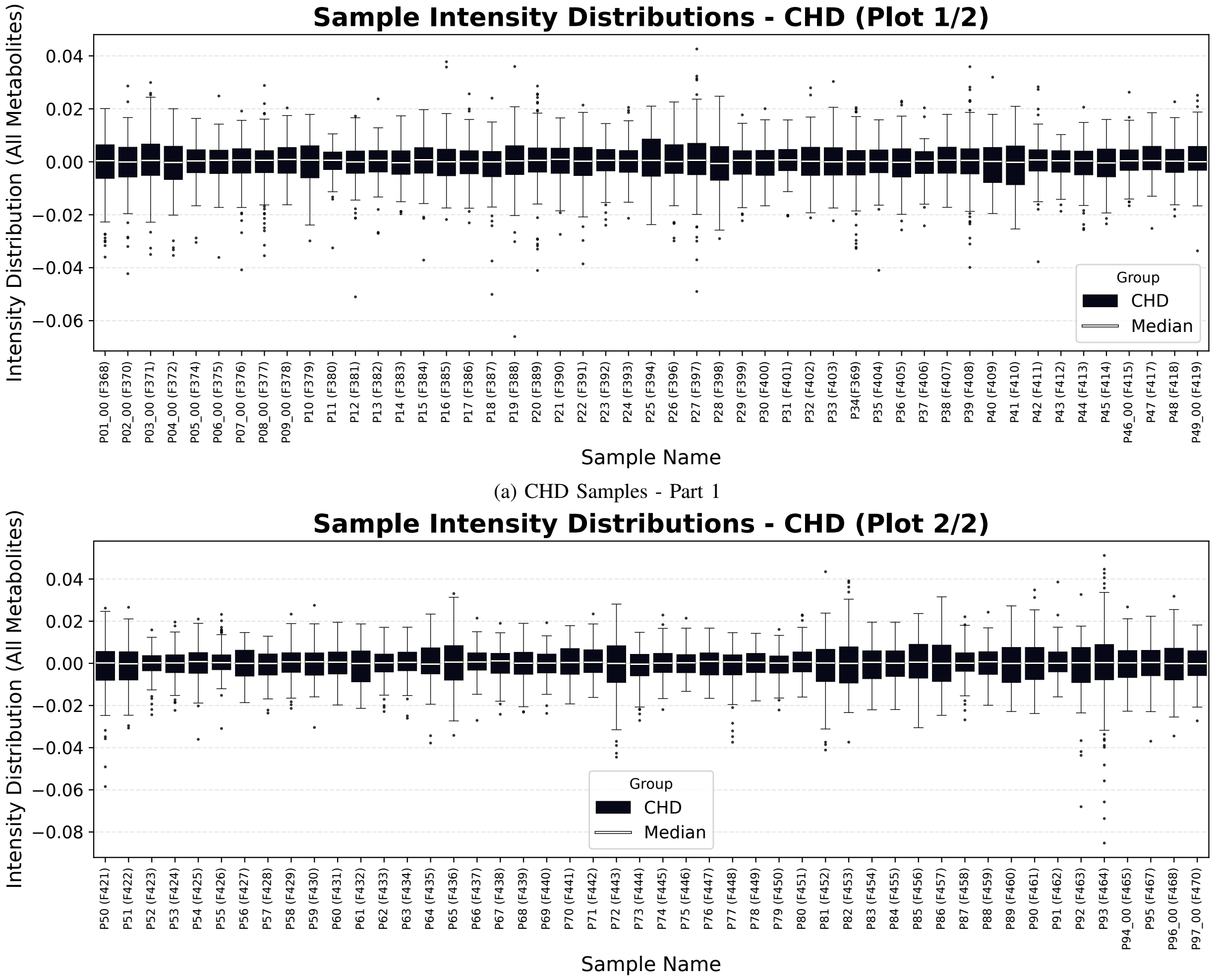

(a) CHD Samples - Part 1

(b) CHD Samples - Part 2

Fig. 16: **Intensity Distributions of CHD Samples.** Used to verify the consistency of pathological samples before removal.

e) Final Dataset Re-Processing and Validation

Following the removal of the identified outliers, the dataset was re-processed from the ground up. This step is critical: removing samples alters the global parameters (mean, standard deviation, Frobenius norm) used for Normalization, Autoscaling, and Block Scaling. Therefore, to ensure mathematical rigor, the remaining samples were re-normalized and re-scaled independently in their respective blocks (ESI- and ESI+) before being fused again.

A final PCA was performed on the cleaned and re-fused dataset (Figure 17) to verify the data structure. The Score Plot (b) shows a more homogeneous distribution without the compressing effect of extreme outliers. The Scree Plot (a) confirms a balanced variance distribution, and the Loading Plot (c) highlights that the separation is now driven by relevant biological features (e.g., C8-Carnitine, Indole derivatives) rather than technical artifacts. This curated dataset constitutes the input for the subsequent Data Splitting and Classification phases.

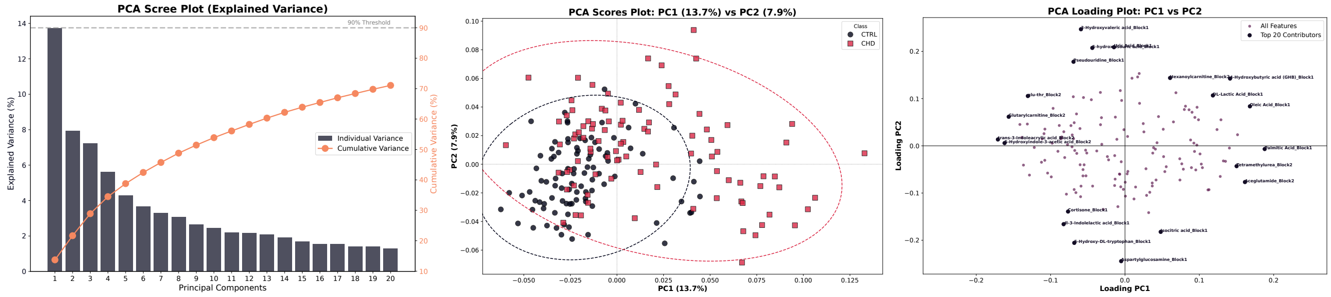

(a) Final Scree Plot (b) Final Score Plot (c) Final Loading Plot

Fig. 17: **PCA of the Curated Fused Dataset (Post-Outlier Removal).** (a) Variance is well-distributed. (b) Samples are homogeneously distributed in the score space, with no extreme outliers distorting the axes. (c) Loadings confirm the contribution of relevant biological markers (e.g., Acylcarnitines, Indoles) to the data variance.

2.6 Dataset Splitting and Prevention of Data Leakage

To ensure an unbiased estimation of the predictive models' performance, a rigorous data splitting protocol was implemented. A critical challenge in multi-block analysis (Low-Level Fusion) is preserving the independence of the test set throughout the entire pre-processing chain. Performing operations such as Autoscaling or Block Scaling on the entire dataset prior to splitting would introduce **Data Leakage**, as the training set would effectively ”see” information regarding the distribution of the test set (e.g., global mean or variance), leading to overly optimistic results.

a) Anti-Leakage Workflow

To address this, we adopted an index-based splitting strategy. The indices for Training and Test sets were generated on the raw concatenated data to ensure that the same biological samples were assigned to the same partitions across both ESI+ and ESI- blocks. Subsequently, the following pipeline was executed independently for each fold/split:

1) **Splitting:** The raw ESI+ and ESI- blocks were physically separated into Training and Test sets using the pre-calculated indices.
2) **Independent Pre-processing:** Normalization (PQN) and Transformation (Log10) were applied. Since these are sample-wise operations, they do not cause leakage.
3) **Learned Autoscaling:** The mean (μ_{train}) and standard deviation (σ_{train}) were calculated *exclusively* on the Training set. The Test set was then scaled using these learned parameters: $X_{test,scaled} = (X_{test} - \mu_{train})/\sigma_{train}$.
4) **Learned Block Scaling:** The Frobenius norm ($||X||_F$) was computed on the scaled Training block. Both Training and Test blocks were then divided by this training-derived scalar.
5) **Concatenation:** Only at this final stage were the blocks fused, ensuring that the Test set remained a strictly unseen entity.

b) Splitting Methodologies

Three distinct splitting algorithms were compared to evaluate model robustness under different conditions:

- **Random K-Fold Cross-Validation ($k = 5$):** Used as a baseline to evaluate the impact of chance. Samples are assigned randomly without constraints.
- **Stratified K-Fold Cross-Validation ($k = 5$):** The gold standard for clinical datasets. It ensures that the proportion of classes (CHD vs CTRL) is preserved in every fold, preventing bias due to class imbalance.
- **Duplex Algorithm (Split 75/25):** A deterministic method designed to cover the experimental space. Unlike random selection, Duplex uses Euclidean distances (calculated on PCA scores explaining 95% variance) to iteratively select the most distant samples for both Training and Test sets. This ensures that the Test set includes ”extreme” samples, providing a rigorous assessment of the model's interpolation and extrapolation capabilities.

c) Evaluation of Splits

The characteristics of the generated splits were analyzed in terms of Class Balance Discrepancy (deviation from the original class ratio) and Spatial Distance Ratio (ratio of average distance from the center in Test vs Train). The results are summarized in Table V.

As expected, Stratified **K-Fold** maintained the lowest Class Balance Discrepancy (Avg: 2.16%), ensuring ideal training conditions. Conversely, **Random K-Fold** showed high instability (Avg Discrepancy: $\approx$ 12.8%), with some folds significantly under-representing the pathological class. The **Duplex** method, while maximizing spatial coverage (Spatial Dist. Ratio = 1.22, indicating a Test set more dispersed than the Training set), resulted in a higher class imbalance. This behavior is inherent to the algorithm, which prioritizes geometric diversity over label frequencies, creating a challenging ”stress test” for the classifiers.

2.7 Statistical and Machine Learning analysis

Following the rigorous data splitting protocol, the study proceeded to the critical phase of model selection and feature discovery. Given the high-dimensional nature of the metabolomic dataset ($P \approx N$), the primary methodological challenge was

TABLE V: Comparison of Dataset Splitting Strategies. Values for K-Fold methods are reported as the average across the 5 folds.

Strategy	**Class Balance Discrepancy (%)**	**Train Prop. CHD (%)**	**Test Prop. CHD (%)**	**Spatial Dist. Ratio (Test/Train)**
Random CV (Avg)	12.86	49.7	49.7	1.01
Stratified CV (Avg)	**2.16**	**49.8**	**49.7**	**1.02**
Duplex (75/25)	31.97	45.7	61.7	**1.22**

to identify a modeling architecture capable of discerning true biological signatures from background noise without succumbing to overfitting.

Initial screenings performed on the Random and Duplex splits revealed a potential pitfall: complex non-linear algorithms, such as Random Forest and Support Vector Machines, exhibited near-perfect performance on training data but failed to generalize consistently on the geometric ”stress-test” provided by the Duplex split. This observation necessitated a shift towards regularized linear models, which prioritize parsimony and interpretability. Consequently, the analysis focused on two complementary algorithms: **Logistic Regression with Lasso (L1) penalty** and **Partial Least Squares Discriminant Analysis (PLS-DA)Train Prop.**.

The final variable selection and classification were conducted using the **Stratified K-Fold** scheme to ensure statistical stability across iterations.

a) Algorithmic Implementation

The strategy relied on the specific strengths of the selected models:

- **Lasso Logistic Regression:** Configured with a regularization parameter $C = 50$, the model acted as a mathematical filter. The L1 penalty forces the coefficients of non-informative variables to zero, effectively selecting a sparse subset of features necessary for classification.
- **PLS-DA Optimization:** As the chemometric gold standard, PLS-DA was used to model the global variance. For each fold, the number of Latent Variables (LVs) was optimized iteratively (testing 1 to 10 LVs) to minimize the classification error without introducing unnecessary complexity.

b) Model Validation

To rule out chance correlations, the PLS-DA model underwent a rigorous **Permutation Test** (100 iterations). The results (Figure 18d) showed that the model’s accuracy was significantly higher than any distribution generated by random label shuffling, yielding a p-value of 0.0099, confirming the statistical validity of the observed separation.

c) Performance Visualization (Fold 1)

Figure 18 illustrates the PLS-DA performance for a representative fold (Fold 1). The Optimization Curve (c) shows a sharp decrease in error, stabilizing at the optimal number of components. The Score Plot (a) demonstrates a clear separation between CHD and CTRL groups in the latent space, driven by the metabolites identified in the Loading Plot (b). The Predicted vs. Observed plot (e) confirms the robustness of the decision boundary, with minimal misclassification.

d) Consensus Variable Selection

To define the final panel of potential biomarkers, a consensus strategy was adopted. Variables were selected only if they satisfied two strict criteria simultaneously: (1) retention by the Lasso algorithm (non-zero coefficient) indicating predictive necessity, and (2) high importance in the PLS-DA model (Variable Importance in Projection, VIP score > 1.5) indicating dominance in variance explanation. This intersection approach yielded a robust signature of 8 metabolites, comprising contributions from both the Negative (Block 1) and Positive (Block 2) ionization modes:

- **Block 1 (ESI-):** 4-Hydroxybutyric acid (GHB), 5-Hydroxy-DL-tryptophan, DL-Lactic Acid, Linoleamide, Palmitic Acid.
- **Block 2 (ESI+):** Acetyl-L-carnitine, L-Cystine, Myristamide.

These features represent the core metabolic alterations identified by the study and will be the subject of the biological interpretation in the following chapter.

2.8 Software and Technological Stack

The entire analytical ecosystem was developed within the **Python** programming environment, selected for its extensive support for data science and bioinformatics research. To ensure the full reproducibility of the study, specific libraries were employed to handle the distinct phases of the pipeline, from data manipulation to statistical modeling and visualization.

a) Data Management and Computation

The organization and manipulation of the high-dimensional metabolomic datasets were managed using **Pandas**. This library provided the essential DataFrame structures required for data cleaning, filtering, and the alignment of samples across the different analytical blocks. **NumPy** was utilized for high-performance vector integration and complex array operations, serving as the computational engine for mathematical tasks such as covariance matrix calculations and the derivation of VIP scores.

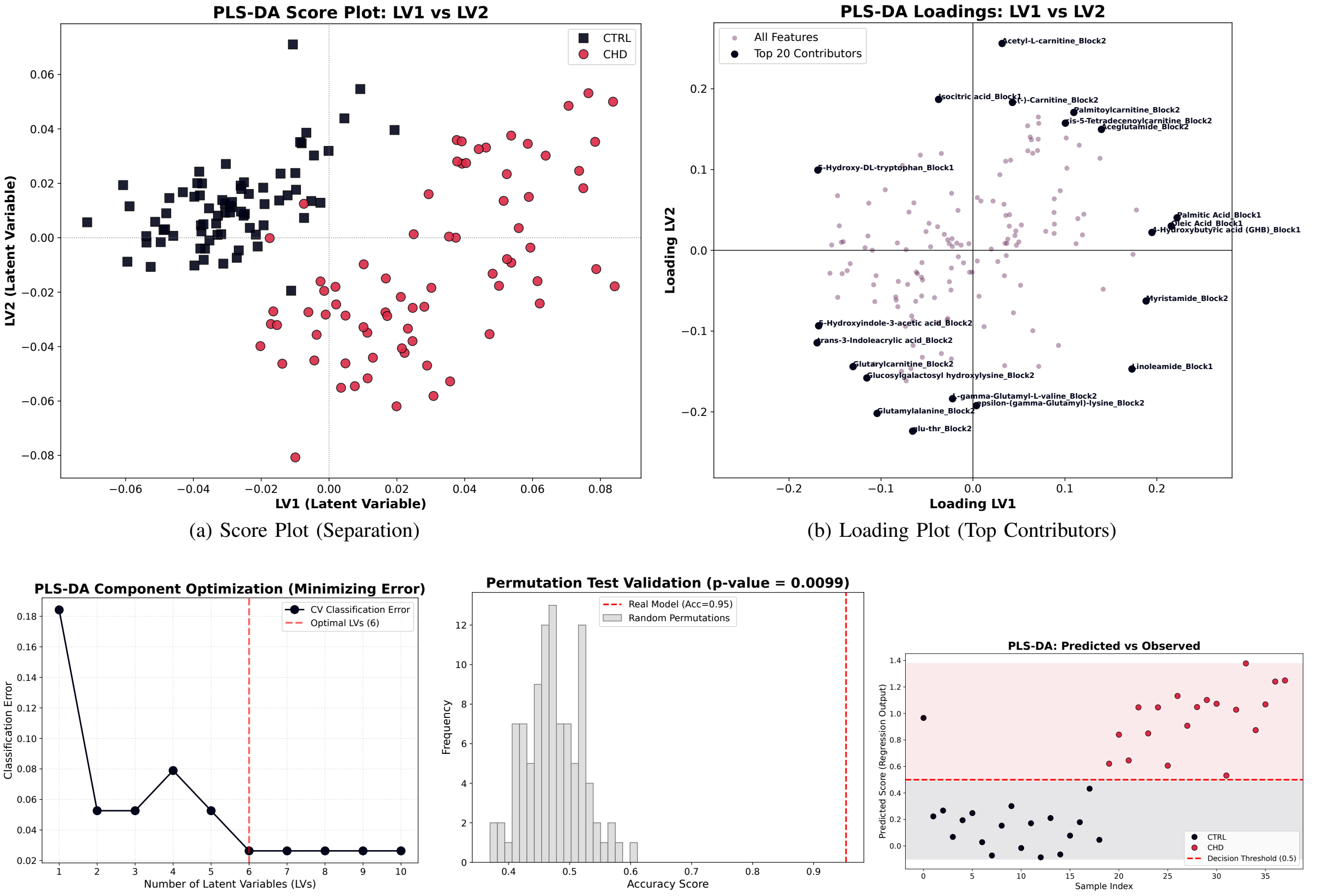

(a) Score Plot (Separation)

(b) Loading Plot (Top Contributors)

(c) LV Optimization

(d) Permutation Test ($p = 0.0099$)

(e) Predicted vs Observed

Fig. 18: **PLS-DA Model Performance and Validation (Representative Fold 1).** (a) Clear clustering of CHD vs CTRL in the latent space. (b) Top 20 features driving the separation, highlighting contributions from both blocks (e.g., Myristamide, Palmitic Acid). (c) Selection of optimal Latent Variables minimizing error. (d) Permutation test confirming the model is not overfitting (Real accuracy ¿ Random distribution). (e) High classification accuracy on the test set.

b) Machine Learning and Statistical Analysis

The algorithmic core of the project relies on **Scikit-learn**, the standard library for machine learning in Python. This toolkit was utilized extensively across the pipeline, specifically for:

- **Pre-processing:** Encoding of categorical variables (via LabelEncoder) and data scaling.
- **Modeling:** Implementation of predictive algorithms, including Logistic Regression (L1-Lasso regularization), Support Vector Machines (SVM), Random Forest, and Partial Least Squares Discriminant Analysis (PLS-DA, adapted via the `PLSRegression` module).
- **Validation:** Execution of the rigorous validation protocols, including Stratified K-Fold Cross-Validation, calculation of performance metrics (AUC-ROC, Accuracy, Sensitivity, Specificity), and the implementation of Permutation Tests to assess statistical significance.

c) Scientific Visualization

Graphical interpretation of the results was achieved through the integration of **Matplotlib** and **Seaborn**. Matplotlib was employed for the fundamental graphical architecture and the rendering of advanced geometric elements, such as the 95% confidence ellipses in the Score Plots. Seaborn complemented this by generating high-level statistical visualizations, including Loading profiles, Permutation histograms, and Feature Importance rankings, ensuring a clear and professional aesthetic suitable for academic publication. Finally, the **OS** module facilitated automated file management and directory structuring, guaranteeing the portability of the code and the organized storage of results.

3 Results and Discussion

The final phase of the study focused on the validation and interpretation of the identified metabolic signature. Having selected a consensus panel of 8 potential biomarkers through the intersection of Lasso regression and PLS-DA VIP scores, a series of targeted analyses were conducted to verify their discriminatory power and statistical robustness independent of the complex multivariate models used for their discovery.

3.1 Univariate Statistical Validation

As a first step, the statistical significance of each selected feature was assessed individually. A Welch's t-test (unequal variance) was performed comparing the intensity levels between CHD and Control groups. To control for the risk of false positives inherent in multiple hypothesis testing, the resulting p-values were corrected using the Benjamini-Hochberg False Discovery Rate (FDR) procedure.

The results confirmed that all 8 metabolites are highly significant potential markers. Specifically, features such as **Myristamide** and **L-Cystine** exhibited extremely low adjusted p-values ($p_{adj} < 10^{-20}$), indicating a probability close to zero that the observed differences are due to chance. Other key metabolites, including **Linoleamide** and **Palmitic Acid**, also showed strong statistical significance ($p_{adj} < 10^{-10}$), reinforcing their role in the metabolic alteration associated with the pathological condition. The consistency of these univariate results provides a solid independent validation of the multivariate selection process.

3.2 Multivariate Confirmation of the Reduced Panel

To verify whether the simplified panel of 8 metabolites retained sufficient information to distinguish the clinical groups, a final Principal Component Analysis (PCA) was performed using exclusively these features. This ”stress test” aimed to answer a critical question: *can we reduce the complexity from hundreds of variables to just 8 without losing the ability to stratify patients?*

The results are presented in Figure 19. The Score Plot (b) demonstrates that the separation between CHD (orange) and CTRL (blue) remains remarkably clear and distinct along the first principal component. This confirms that the selected subset captures the core biological variance of the dataset. The Loading Plot (c) further highlights the contribution of each marker to this separation, with metabolites like **Acetyl-L-carnitine** and **L-Cystine** showing strong loadings, while the Scree Plot (a) indicates that the first two components explain a substantial portion of the total variance (approx. 60%), suggesting a high information density in the selected panel.

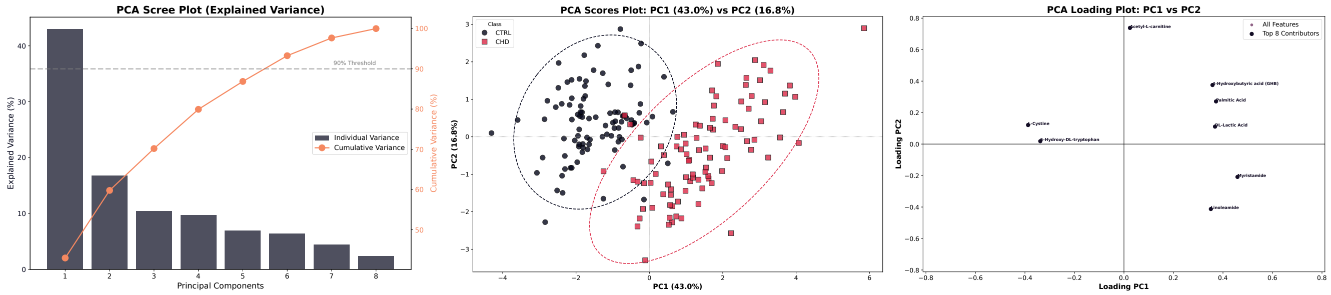

(a) Explained Variance

(b) Final Score Plot (8 Features)

(c) Loading Plot (Feature Contribution)

Fig. 19: **PCA Validation of the 8-Biomarker Panel.** (a) The scree plot shows that the reduced dataset retains significant variance. (b) The clear separation between CHD and CTRL groups confirms that the 8 selected features are sufficient to capture the biological distinction. (c) Loadings indicate the strong contribution of markers like Acetyl-L-carnitine and L-Cystine to the model.

3.3 Distributional Analysis

To visualize the behavior of the individual markers, boxplots of the intensity distributions were generated (Figure 20). This graphical inspection reveals distinct trends: metabolites such as Myristamide and Linoleamide show a clear upregulation or downregulation trend in the pathological group compared to controls. The tight interquartile ranges in several features further suggest that these alterations are consistent across the population and not driven by outliers.

3.4 Predictive Power Assessment

The definitive validation involved training a PLS-DA classifier using *only* the 8 selected potential biomarkers. To ensure a realistic performance estimate, the model was evaluated via Stratified 5-Fold Cross-Validation. Crucially, the entire pre-processing pipeline (Autoscaling and Frobenius Block Weighting) was re-learned within each fold loop, preventing any data leakage. The model achieved an exceptional average accuracy of approximately **97%** on the test sets. This result demonstrates that transitioning from a complex profile of hundreds of variables to a simplified panel of 8 key metabolites not only maintains

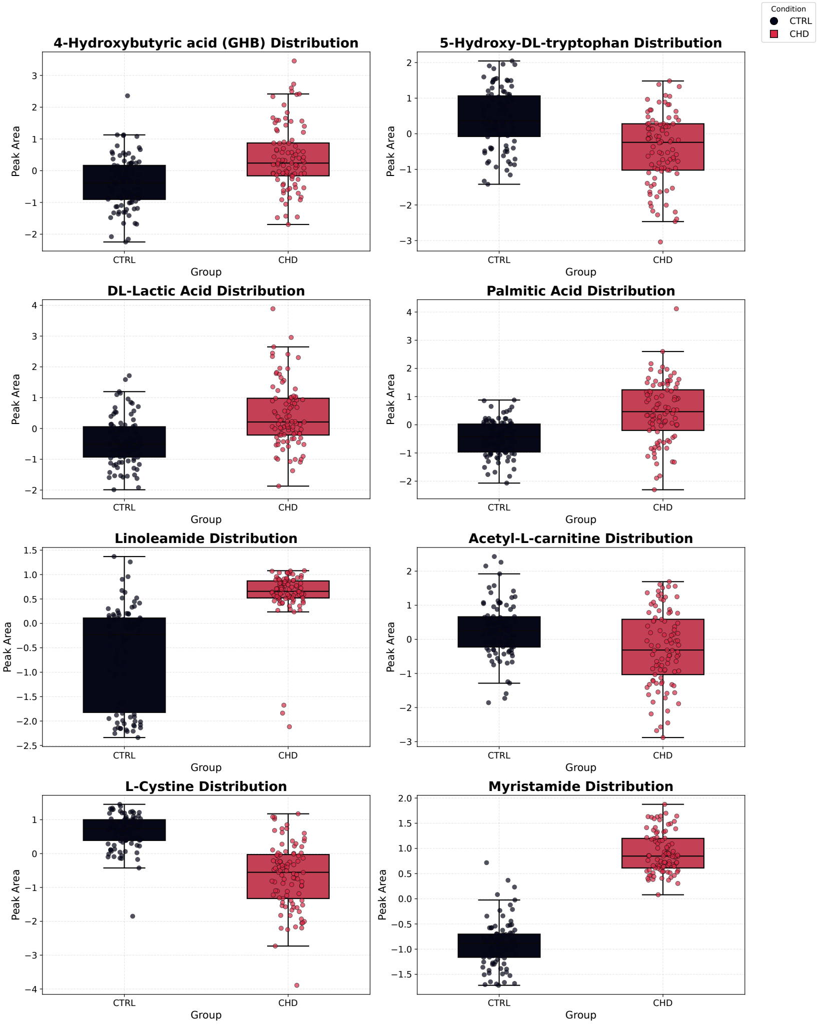

Fig. 20: **Intensity Distributions of the Selected Potential Biomarkers.** Boxplots comparing the normalized intensities of the 8 potential biomarkers in Control (CTRL) vs Disease (CHD) groups. Clear shifts in median values are observable, corroborating the univariate statistical significance.

diagnostic power but potentially enhances the robustness and interpretability of the model, making it a viable candidate for future clinical translation.

It is important to emphasize that while these results are statistically robust, the identified features should be considered **potential** biomarkers. A deeper biological validation is required to confirm their causal role in the pathology.

4 Conclusions

This project presented a comprehensive computational workflow for the analysis of untargeted metabolomics data, aiming to identify potential biomarkers distinguishing Congenital Heart Disease (CHD) subjects from healthy controls. The study moved beyond a rigid, standard pipeline, adopting instead a flexible and iterative approach where every methodological choice—from data cleaning to model selection—was driven by a critical evaluation of the results. The extensive use of visualization tools, such as PCA score plots and diagnostic boxplots, proved instrumental in guiding decisions, particularly in the complex phases of normalization and anomaly detection.

The integration of ESI+ and ESI- data via Low-Level Data Fusion, combined with a rigorous outlier detection strategy based on the consensus of statistical and machine learning algorithms, allowed for the construction of a high-quality dataset. The subsequent feature selection process, leveraging the complementarity of Lasso regression and PLS-DA, successfully narrowed down the high-dimensional space to a panel of 8 statistically significant metabolites. These features demonstrated a remarkable ability to classify the subjects, achieving high predictive accuracy while ensuring model parsimony.

However, as an exploratory work, this study has several limitations that outline directions for **future developments**:

- **Data Fusion Strategies:** We focused exclusively on Low-Level Fusion. Future works could explore Mid-Level (feature level) or High-Level (decision level) fusion to evaluate if different integration strategies yield complementary insights.

- **Modeling Alternatives:** While we employed discriminative models, class-modeling techniques like SIMCA (Soft Independent Modeling of Class Analogy) could be tested to better characterize the ”normal” metabolic space.
- **Advanced Splitting and Augmentation:** Splitting strategies based on clustering could ensure an even more rigorous separation of biological variability. Furthermore, techniques of data augmentation (e.g., SMOTE for metabolomics) could be investigated to improve model robustness on small cohorts.
- **Refined Tuning:** The anomaly detection phase could benefit from a sensitivity analysis on the contamination parameters, and the univariate analysis could be expanded with Volcano plots and Heatmaps for a richer graphical representation.
- **Biological Validation:** Most importantly, the biological interpretation of the identified markers was limited. A collaboration with clinical experts and pathway analysis would be essential to translate these statistical findings into meaningful pathophysiological insights.

In conclusion, while acknowledging its limitations, this work demonstrates that a rigorous, data-driven approach can effectively extract meaningful information from complex omics data, providing a solid foundation for future biomarker discovery research.

References

[1] Mires, Stuart, et al. ”Plasma metabolomic and lipidomic profiles accurately classify mothers of children with congenital heart disease: an observational study.” Metabolomics 20.4 (2024): 70.

[2] De Livera Alysha, M., et al. ”Normalizing and Integrating Metabolomics Data.” (2012).

[3] Psychogios, Nikolaos, et al. ”The human serum metabolome.” PloS one 6.2 (2011): e16957.